Biotribology 3 (2015) 1–10

Contents lists available at ScienceDirect

Biotribology

journal homepage: http://www.elsevier.com/locate/biotri

Tribology of particle suspensions in rolling-sliding soft contacts

G.E. Yakubov [a,b,c,*], T.E. Branfield [c,1], J.H.H. Bongaerts [c,2], J.R. Stokes [a,b,c,*]

[a] School of Chemical Engineering, The University of Queensland, Brisbane 4072, Australia
[b] Australian Research Council Centre of Excellence in Plant Cell Walls, The University of Queensland, Brisbane 4072, Australia
[c] Unilever Discover, Unilever R&D Colworth, Colworth House, Sharnbrook, Bedford MK44 1LQ, United Kingdom

ARTICLE INFO

Article history:
Received 11 November 2014
Received in revised form 13 August 2015
Accepted 13 September 2015
Available online 16 September 2015

Keywords:
Particles
Suspensions
Soft tribology
Biolubrication
Biotribology
Food

ABSTRACT

We investigate the lubrication of microsphere suspensions between compliant substrates, and probe the influence of matrix viscosity, particle phase volume, surface roughness and wetting, and slide-to-roll ratio (SRR). In general, the suspensions behave as a continuum in the elastohydrodynamic regime provided the film thickness, which is predicted from the product of speed and viscosity, is greater than the particle diameter. Below this, the frictional response is characteristic of the mixed and boundary regimes. In the boundary regime, friction is independent of phase volume above 5% and it is governed by the rolling friction associated with particles being entrained into the contact that is independent of SRR, which is made possible by substrate deformation. This study provides a benchmark for soft-tribology and biotribology studies involving more complex particle suspensions and particle-containing soft materials.

1. Introduction

There has been a recent surge of interest in the soft-contact tribology and elastohydrodynamic lubrication due its application in the biotribological contacts present during oral processing of food and oral care products as well as during rubbing of personal care products to skin and hair [1–3]. Solid particles are added to consumer products for a variety of reasons, which includes improving the sensory feel of skin creams [4] and food products [5]. They can also be particle suspensions by nature; for example, molten chocolate is a suspension of cocoa bean plant cell wall particles in a continuous fat phase [6,7]. While there is increasing use of tribology to study the properties of foods, and attempts to relate these to texture perception, the presence of particles makes it challenging to interpret measured lubrication properties. In addition, the bulk rheological properties of a particle suspension as well as individual particle properties such as hardness, morphology, size and surface potential, are likely to influence lubrication and surface wear during rubbing contacts, as well as texture perception. To assist in elucidating the dynamic response of consumer product systems that contain particulates, we investigate the lubricating behaviour of model suspensions containing non-colloidal glass spheres in viscous aqueous solutions within a compliant elastomer contact.

Microparticles are increasingly used purposefully as additives for soft contact lubricants to reduce friction and minimise erosion [8–10]. The addition of particles to a system modifies rheology (e.g. viscosity, fluid elasticity) and can minimise adhesive interactions between surfaces that are otherwise liable to stickiness. Elastomer particles are purposefully added to skin creams to improve sensorial perception [4,11] and creating a so-called 'silky' feel. The presence of particles affects the sensory properties of food systems that depends on particle size, hardness and phase volume. For example, 'creaminess' texture can be enhanced by the presence of particles when their size is in the range of 0.1–3 μm diameter, while large hard particles lead to 'grittiness' [12,13]. In another example, starch granules have been used successfully as fat replacer in mayonnaise, but while these can maintain the rheology of the product upon fat reduction, 'gritty' after-feel has also been observed that may be associated with the presence of hard particles [12–14]. In biolubrication, such as cartilage and oral salivary lubrication, the presence of particulates is often associated with physiological changes in response to mechanical exertion, fatigue, tooth attrition, periodontal disease or consumption of certain foods or beverages [15].

Despite the obvious importance of understanding and characterising the lubricating properties of particle-laden fluids in soft-tribological contacts, there are only a few tribological studies on such systems [1,16]. Based on more extensive studies using hard tribological contacts, it has been established that the lubrication regime has a major influence on how particles affect lubrication and wear. It has been shown that the particle size/film thickness ratio is critical for particle entrainment, with

* Corresponding authors at: School of Chemical Engineering, The University of Queensland, Brisbane 4072, Australia.
E-mail addresses: Gleb.Yakubov@uq.edu.au (G.E. Yakubov), Jason.Stokes@uq.edu.au (J.R. Stokes).
[1] Current address: Bristol Centre for Functional Nanomaterials, Centre of Nanoscience and Quantum Information, University of Bristol, Tyndall Avenue, Bristol, BS8 1FD, United Kingdom.
[2] Current address: SKF Engineering and Research Centre, Nieuwegein, The Netherlands.

http://dx.doi.org/10.1016/j.biotri.2015.09.003
2352-5738/

nanoparticles for example only moving through a rolling/sliding contact when their size is less than the film thickness [17–19]. The slide–roll ratio (SRR) is reportedly important: high rolling conditions act to entrain particles through a contact whereas high sliding settings lead to particle accumulation and subsequent dispersant starvation [9,17,20]. Also notable is the geometry of the contact and its surface roughness; wedge-shaped rolling/sliding contacts act to engulf particles [9,17,21] and rougher surfaces assist entrainment of particles [22–24]. The hydrodynamics of the inlet zone have an effect; for example, the position of emulsion droplets in the inlet determines whether they flow away or get drawn into the contact [25]. We focus here on soft contact tribology that presents some essential difference to hard tribological contacts. In the compliant rolling/sliding contact, deformation of the substrates cannot be neglected and the contact pressures are much lower compared to hard contacts. In addition, the components of rolling friction arising from elastic hysteresis are of comparable magnitude to sliding friction [26,27]. In addition, the area of contact between the soft tribopairs investigated here is of order 1000 times greater than for hard tribopairs (e.g. steel); i.e. ~8 mm^2 versus ~0.005 mm^2 respectively. We thus anticipate for particle-mediated lubrication between elastic substrates that: (i) high rolling conditions (i.e. low SRR) promote entrainment of particles into the gap; (ii) high sliding conditions (i.e. high SRR) promote particle accumulation outside the contact [9]; and (iii) substrate deformation promotes entrainment of hard particles into the contact.

To begin disentangling rheological and particle dynamics effects in soft contacts, we investigate the lubricating properties of model suspensions in a compliant contact formed by polydimethylsiloxane (PDMS) ball and plate in a rolling/sliding contact. The PDMS is chosen because its surface properties (e.g. surface roughness, hydrophobicity) are easily altered and because it is commonly used to mimic bio-surfaces. The experiment utilises model two-phase lubricants consisting of non-colloidal micron-scale hollow glass spheres dispersed in density matched viscous Newtonian fluids free from polymer and/or surfactant additives, which enables construction of full Stribeck curves under fully flooded conditions. These spherical particles are non-adhesive with essentially hard wall interaction potential and minimal inter-particle interaction forces that drive aggregation. Our aim is to stimulate further research by providing systematic experiments exploring the phenomenon of third body lubrication in soft tribological contacts, and to provide a benchmark for studies on more complex multiphase fluids common in foods and personal care products.

2. Materials and method

2.1. Friction measurements

The friction measurements are performed using a Mini Traction Machine (MTM, PCS Instruments Ltd., UK). The rubbing contact consists of a polydimethylsiloxane (PDMS) (SYLGARD® 184 Silicon Elastomer Kit, Dow Corning, MI) ball of radius 0.95 cm and PDMS disc of radius 23 mm and thickness 4 mm, fully immersed in lubricant. As in a previous study [3], discs are used with three surface roughness values: 'smooth' with a root-mean-square (RMS) roughness of 9 nm, 'medium rough' with an RMS roughness of 380 nm and 'rough' with a RMS roughness of 3.6 μm. The PDMS ball has only one surface RMS roughness at 26 nm. The Young's modulus of the PDMS is 2.4 MPa [3]. Untreated hydrophobic PDMS surfaces were used unless stated otherwise. For some experiments, PDMS was made hydrophilic using oxygen plasma treatment (Cressington Carbon Coater, 208 Carbon). The samples are held in a vacuum at a vapour pressure of 0.2 mbar, and a current of 15 mA is applied for 99 s. Exposed to air, this applied hydrophilicity reduces over time; the samples are therefore stored in water immediately after treatment and used at once.

In a typical MTM experiment, the ball and disc are driven independently at velocities v_b and v_d respectively, yielding the entrainment speed $U = (v_b + v_d)/2$. The relative motion of the moving ball and disc determine the slide-to-roll ratio, $SRR = (v_b - v_d)/U$. The lateral friction force F_i experienced by the ball is measured using a force transducer. To prevent offset errors, lateral force measurements are taken at each entrainment speed when $v_b > v_d$ and $v_b < v_d$, both rotating in the same direction, and the average was taken. As rolling friction F_r does not change sign when the relative motion of the disc and ball is reversed, this yields only the sliding friction, which is presented for most experiments. To be able to measure the total friction and separate the sliding component from the rolling component of the friction, in some measurements the ball and the disc speeds are also reversed. This gives four friction measurements at each entrainment speed, when $_b$ and v_d are both negative and both positive and with one larger than the other as given in de Vicente et al. [26]. Combining these measurements allows the determination of the rolling friction (F_r) and sliding friction (F_s). Further details of the rolling and sliding friction in PDMS soft contact are also presented elsewhere [3].

A load, L, is applied onto the ball and the normal force is measured using a strain gauge installed on the leaf spring of the MTM. The lateral friction force, F_f, and the normal load yield the friction coefficient, $\mu = F_f/L$.

One way of representing friction in different lubrication regimes is using a so-called Stribeck curve, in which the friction coefficient is plotted against the product of U and the viscosity of lubricant in the contact, η_c. For each entrainment speed, at a constant SRR, five friction measurements are taken and averaged. To test for hysteresis, each entrainment speed is tested twice in the same experiment; measurements are first taken from the highest speed 750 mm/s and the speed is step-wise decreased to the lowest speed of 1 mm/s, after which the speed is increased again to 750 mm/s. Other experiments were performed at constant speed at a varying load L or varying SRR.

2.2. Suspension preparation and characterisation

The test solutions are suspensions of hollow glass spheres (Omya UK Sphericel 110P8) dispersed in Newtonian fluids of different viscosity, enabling a full Stribeck curve to be constructed. Spheres are specified to have a mean diameter of 9 μm. The particle size distributions are determined using static light scattering on a Malvern Mastersizer. The spheres have a volume weighted mean diameter $D(4.3) = 8.94$ μm, with 10% of the particles below $D(0.1) = 4.10$ μm and 90% of the particles below $D(0.9) = 15.07$ μm.

The hollow glass spheres have a mean specific gravity of 1.1 g/cm^3, similar to that of the dispersant liquid used. Hollow spheres are chosen because they sediment/cream much more slowly than solid spheres that readily sediment. However, it is perhaps important to note that the lower mass of the hollow glass spheres compared to solid glass spheres may result in different tribological properties, due to their lower inertia. The particle volume fractions employed are 0%, 10%, and 45%. These are dispersed in a range of fluids: water (filtered and demineralised), 95 wt.% glycerol in water and 90 wt.% corn syrup in water. In order to make suspensions of a certain phase volume, the densities of the particle-free 95 wt.% glycerol and 90 wt.% corn syrup were evaluated using an Anton Paar DMA 35N density meter, and were found to be 1.25 g/cm^3 and 1.38 g/cm^3, respectively. The suspensions are gently stirred immediately before measurements to distribute the spheres uniformly throughout the solution.

The viscosities of the test fluids have been measured on an AR2000 rheometer (TA Instruments). The temperature is set a constant 23 °C and parallel plate geometry is used with a 40 mm diameter smooth aluminium plate. Parallel plate geometry was chosen to enable gap-dependent effects on the viscosity to be assessed as well as obtain high shear rates following Davies and Stokes [28,29]. The shear stress is varied from 0.1 Pa to 10^4 Pa and the fluids were found to be Newtonian. Corrections to the viscosity are performed to remove any gap error in the rheometer plate setup, as described in Davies and Stokes [28,

Table 1
Measured viscosities (AR2000 rheometer, 40 mm parallel plate) of the lubricating fluids utilised in this work. All fluids and suspensions are Newtonian.

Particle phase volume ϕ	Dispersant	Viscosity (mPas)
Matrix fluids		
0%	Water	1
	95 wt.% glycerol/water	365
	90 wt.% corn syrup/water	1320
Suspensions		
10%	Water	1.5
45%	Water	3.5
10%	95 wt.% glycerol/water	400
45%	95 wt.% glycerol/water	3000
10%	90 wt.% corn syrup/water	2120
45%	90 wt.% corn syrup/water	15400

29]. The resulting viscosities are given in Table 1. These measured viscosities agree closely with predictions from the Quemada model [30,31].

2.3. Fabrication of stained PDMS surfaces and confocal scanning laser microscopy imaging

For the dye transfer experiments we used a rubbing contact comprising a PDMS disc (as above) and a PDMS/toluene ball stained with 9,10-diphenylanthracene. To prepare a PDMS/toluene ball, the PDMS elastomer was mixed with the curing agent in a 10:1 ratio and stirred manually for ~10 min. A 0.4 wt.% solution of 9,10-diphenylanthracene (Sigma-Aldrich) in toluene (LabTek) was mixed with PDMS resin in a ratio 1:3 (25% toluene/dye and 75% PDMS). The mixture was then placed in a vacuum oven to remove all air bubbles, and when bubble free was poured into the aluminium ball-shaped moulds. The PDMS was left in the oven at 70 °C for 3 h to set, and then was kept at RT (24 °C) for additional 48 h prior to use. The choice of the dye, 9,10-diphenylanthracene, was dictated by its solubility in toluene and low chemical reactivity, since it was found that many other dye molecules did interfere with PDMS curing process due to presence of chemically reactive groups. The curing process was chosen to minimise the loss of toluene due to evaporation. Due to toluene's high boiling temperature the set PDMS/toluene fabrications were effectively toluene–PDMS gels. The mechanical properties PDMS/toluene materials were not measured, but it was noted the balls were softer than standard PDMS fabrications. When PDMS–toluene balls were pressed against glass or another PDMS surface, one could observe (under a microscope) a very thin film of stained toluene transferred from the ball to the other surface.

Confocal scanning laser microscopy images were recorded using LSM 710 (Zeiss, Germany). The excitation line used was 405 nm and emission was collected in the region between 430 and 520 nm.

3. Results

3.1. The effect of particle phase volume on suspension lubrication

The influence of 10% and 45% spherical particles on the lubrication of aqueous Newtonian fluids are shown in Fig. 1 for a *medium-rough* PDMS disk at a SRR = 50%; we note that the RMS roughness of the surfaces are much smaller than the average particle size. The Stribeck curves for water and suspensions in water, as shown in Fig. 1(A), are within the mixed ($20 \le U \le 750$ mm/s) and boundary ($U < 20$ mm/s) lubrication regimes. The inclusion of glass particles in water significantly reduces the sliding friction coefficient (μ_s) between PDMS surfaces at speeds of below 200 mm/s. For pure water in the boundary regime, we observe that μ_s increases with increasing entrainment speed. We have reported this previously for rough surfaces [3,32], and attribute it to the deformability of the substrate and adhesion between the hydrophobic PDMS surfaces.

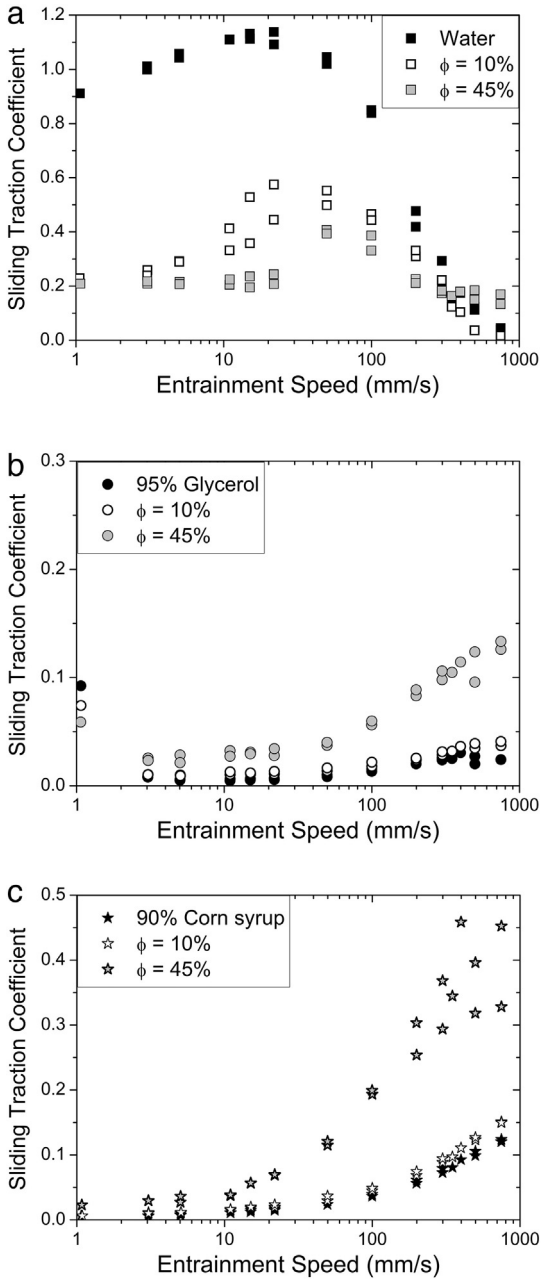

Fig. 1. Stribeck curves for spherical particle suspensions (0, 10%, 45% phase volume) in matrix phase consisting of (a) water, (b) 95/5% glycerol/water mixture, (c) 90%/10% corn syrup/water mixture. The contact consists of hydrophobic PDMS of surface roughness 382 nm.

The two suspensions also exhibit a maximum in μ_s at similar values of entrainment speed to that for water, but there is a more complex dependence on entrainment speed. For $\phi = 45\%$ spheres in water, there is a significant decrease in μ_s as the entrainment speed is decreased from 60 mm/s, and it is then constant at $\mu_s = 0.2$ over the speed range of 20 to 1 mm/s. We also find $\mu_s = 0.2$ at 1 mm/s for the 10% particles suspension. To probe this low-speed regime further, we examine the behaviour with respect to the particle phase volume. Fig. 2 shows that the sliding traction coefficient at an entrainment speed of 5 mm/s decreases with increasing phase volume and is independent of phase volume for 5–45% particles. A reduction in μ_s is apparent even at very low volumes of spherical particles ($\phi = 0.31\%$).

Fig. 1B and C shows the influence of spherical particles on Stribeck curves in the mixed and elastohydrodynamic lubrication (EHL) regimes, which is achieved by dispersing the particles in viscous aqueous

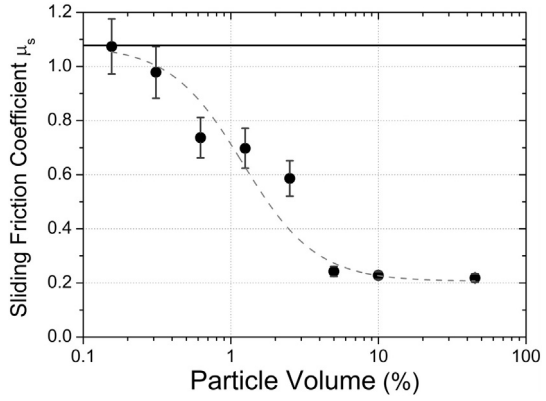

Fig. 2. Sliding friction as a function of particle volume percentage for hard spheres dispersed in water under boundary regime conditions. The contact consists of hydrophobic PDMS of surface roughness 382 nm. The entrainment speed, slide–roll ratio and load are a constant 5 mm/s, 50% and 1N respectively. The solid line represents the PDMS–PDMS friction coefficient in pure water. The dash line is a sigmoidal function drawn to guide the eye.

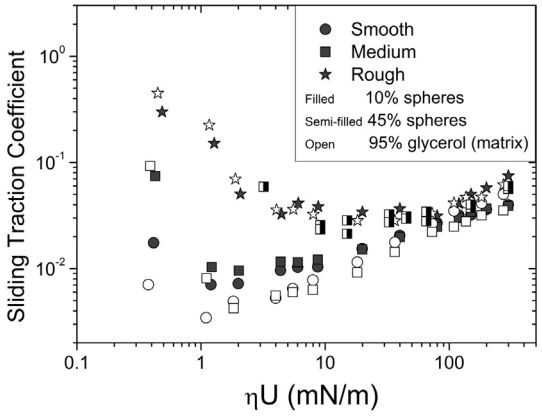

Fig. 4. Stribeck curves for 10% particle suspensions in 95% glycerol/water matrix solvent measured using hydrophobic PDMS contacts of three surface roughnesses; 'smooth', RMS 9 nm; 'medium', RMS 382 nm; 'rough', RMS 3.2 μm. The data for 45% particle suspensions in the same solvent measured using medium rough hydrophobic PDMS contacts is displayed for comparison. The suspension viscosity was used to scale the entrainment speed for systems with particles; solvent viscosity was used for the matrix.

matrices. At the higher speeds, μ_s increases with increasing speed to indicate the EHL regime, and we observe that the inclusion of particles results in higher μ_s compared to the matrix phase alone. These higher values of μ_s are attributed to the increased viscous drag since the bulk viscosity of suspensions increases with increasing phase volume (Table 1).

3.2. The effect of surface roughness on suspension lubrication

The surface roughness of the PDMS tribopair was varied to probe how this may affect particle entrainment. The 10% suspension in water and 95%/5% glycerol/water mixture was investigated between surfaces with three values of RMS roughness; 9 nm ('smooth'), 380 nm ('medium') and 3.6 μm ('rough'). It should be noted that the RMS of 'rough' surface had the same order of magnitude as D(0.1) value of the particles size distribution. The results are summarised in Figs. 3 and 4 respectively; the lines in Fig. 3 are the 'master curves' for water adapted from Bongaerts et al. [3], which we provide as a guide to the previous data generated on a similar set of tribopairs.

For the 'smooth' and 'medium'-rough PDMS surfaces in water (Fig. 3), we observe that the suspension lubricates the same as the matrix phase in the mixed (high speed) regime. As the speed is lowered, the particles have an effect at the transition between mixed and boundary regimes (which we call partial lubrication regime), and in the boundary regime. We find for these two surfaces that the presence of particles lowers the friction in the boundary regime by about four times. In contrast, for the 'rough' surfaces, the particles do not affect the friction measured in the boundary regime, but they do provide a significant reduction in the partial and mixed lubrication regimes.

For the particles in a viscous 95%/5% glycerol/water matrix (Fig. 4), we observe some deviation from the master curve in the EHL regime at low entrainment speeds for the 'smooth' and 'medium-rough' PDMS surfaces, while for 'rough' surfaces the particles did not affect measured friction.

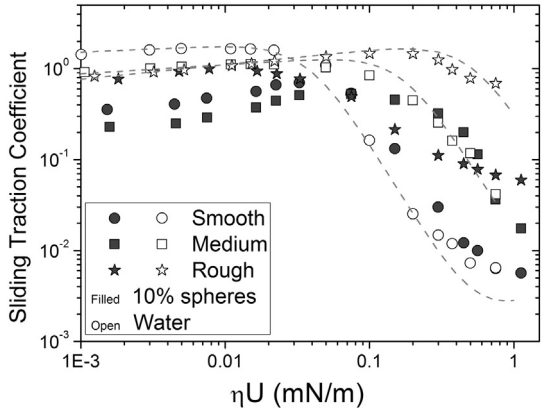

Fig. 3. Stribeck curves for 10% particle suspensions in water measured using hydrophobic PDMS contacts of three surface roughnesses; 'smooth', RMS 9 nm; 'medium', RMS 382 nm; 'rough', RMS 3.2 μm. The dashed lines are the Stribeck curves reported in Bongaerts et al. [3] displayed for reference; the data correspond to particle-free solutions measured using tribopairs with the same values of roughness.

3.3. The effect of slide–roll ratio on suspension lubrication

The influence of slide-to-roll ratio, varying it from pure rolling (SRR = 0%) to pure sliding (SRR = 200%), is shown in Fig. 5 at 5 mm/s which corresponds to the boundary regime. The total friction coefficient for the 45% suspension did not significantly vary with SRR. For the 10% suspensions, the total friction coefficient is constant for SRR < 100%, but then increases with increasing SRR. By contrast, pure water displays similar friction to the suspensions at rolling conditions (SRR < 10%), but increases significantly with increasing SRR and has a much higher friction under sliding conditions.

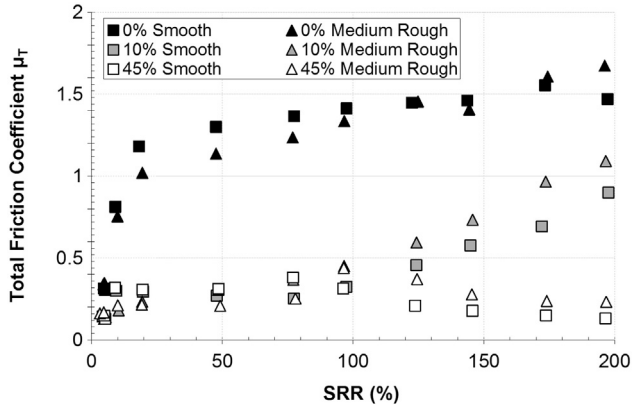

Fig. 5. Total friction coefficient as a function of the slide–roll ratio. The solutions are 0, 10% and 45% micro-spheres in water. The contacts are hydrophobic smooth (RMS 9 nm) and medium rough (RMS 382 nm) PDMS. The entrainment speed is a constant $U = 5$ mm/s.

3.4. The effect of surface hydrophobicity on suspension lubrication

The comparison of Stribeck curves for 10% suspensions in Newtonian fluids for *hydrophilic* and *hydrophobic* PDMS tribopairs is presented in Fig. 6. One can clearly see that presence of particles between hydrophilic surfaces results in the increase of friction in the partial lubrication regime for $\eta U < 0.1$ mN/m, whilst between hydrophobic surfaces they cause a decrease in friction. In the mixed and EHL regimes, the Stribeck curves follow their respective Newtonian counterparts. At very low U, the friction coefficients of the 10% suspensions for both types of surfaces are nearly-identical at ~0.2.

4. Discussion

4.1. The Stribeck behaviour of non-interacting particle suspensions

In order to delineate the influence of viscosity, it is necessary to construct Stribeck curves by multiplying the entrainment speed by the viscosity of the lubricant in the contact zone (η_c). However, η_c is unknown; it depends on the volume fraction of particles being entrained into the contact and the matrix phase viscosity. The phase volume may differ from the bulk suspension if the particles are excluded from the contact zone. We test two cases in Fig. 7; we set η_c to the matrix phase viscosity (η_{matrix}) in Fig. 7(A) and to the bulk suspension viscosity ($\eta_{suspension}$) in Fig. 7(B). These interpretations are compared to the so-called 'master curve' for Newtonian matrices, which is similar to that produced by Bongaerts et al. [3]. Fig. 7 also includes the predicted film thickness (minimum and central) for the EHL regimes calculated using the ηU-based model developed by de Vicente et al. [2,26].

Five regions are observed for the suspensions as the value of $\eta_c U$ and film thickness decreases:

1. EHL regime: suspension is a continuum and friction is defined by $\eta_{suspension}$.
2. EHL-mixed transition: friction deviates from EHL regime when film thickness is similar to particle size or roughness.
3. Mixed lubrication regime: friction increase with decreasing $\eta_c U$.
4. Partial lubrication regime: friction reaches a maximum around $\eta_c U \sim 0.1$ mN/m.
5. Boundary lubrication regime ($\eta_c U < 0.1$ mN/m).

At high speeds, both suspensions fall onto the Master curve in the EHL regime as it can be clearly seen in Fig. 7(B), indicating that this regime is predominantly governed by the suspension viscosity.

With the reduction in the entrainment speed, and thus film thickness, there is a departure from the EHL line that occurs at the same U for 10% and 45% suspensions. This transition may indicate a contribution to the friction response from confinement of the particles in the direction normal to the flow, i.e. the suspension can no longer be treated as homogeneous and particle movement is (vertically) restricted by the shearing surfaces. To examine this EHL-mixed lubrication transition further, we compare 10% suspensions in 95% glycerol (high viscosity) with their Newtonian matrices under conditions of varying surface roughness in Fig. 4. For both 'smooth' and 'medium' rough surfaces, the departure from the matrix curve in the EHL regime occurs at the same entrainment speed (ca. 20 mm/s). The resulting deviation, $\mu_c - \mu_{matrix}$, is of similar magnitude for both surfaces. This similarity can be attributed to the fact that the RMS roughness for both smooth and medium surfaces (RMS ≪ 1 μm) are *significantly* smaller than the average diameter of the particles (D(4.3) = 9 μm). By contrast, for 'rough' surfaces, for which RMS roughness (RMS = 3 μm) is comparable to particle diameter, no difference between suspension and Newtonian solvent (95% glycerol) is observed. The resulting Stribeck curve is characteristic of the EHL - mixed regime transition that occurs for fluid lubricants (see for example, [3,33]) when the film thickness and surface roughness length scales are similar, consequently we can suggest that the vertical confinement produces a similar effect to surface asperities. The latter point can be illustrated by comparing the Stribeck curve recorded in 95% glycerol for the high concentration suspension (45%) between 'medium' surfaces, and its low particle loading counterpart (10%) recorded between 'rough' surfaces. As seen in Fig. 4 both Stribeck curves are nearly identical throughout the EHL-mixed transition, despite difference in sample viscosity.

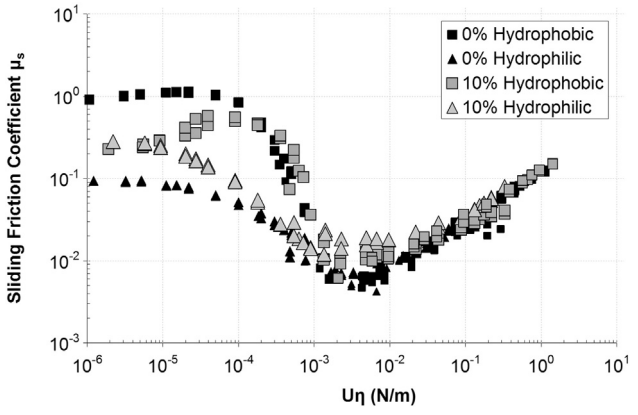

Fig. 6. Stribeck curves of $\phi = 0\%$ and $\phi = 10\%$ glass sphere suspensions in a range of viscous fluids for a hydrophobic and hydrophilic medium rough PDMS contact (RMS 382 nm).

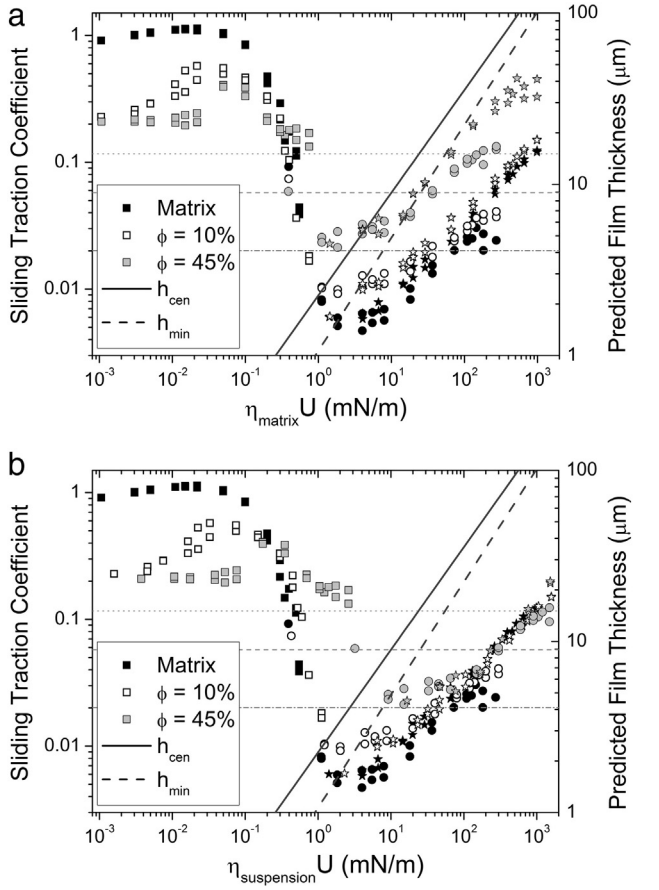

Fig. 7. Stribeck curves for spherical particle suspensions with the entrainment speed multiplied by either the (a) matrix phase viscosity, (b) the suspension viscosity. (a) shows that the Stribeck curve is governed by the matrix phase viscosity in the mixed-regime, while (b) indicates that the suspension rheology governs at high speeds in the EHL regime. The thick lines indicate the predicted film thickness (minimum and central), indicating that the mixed regime is entered for the 45% case when the film thickness is similar to the average particle size. The thin horizontal lines indicate key parameters of particle size distribution; D(0.1) 'dash-dot', D(0.9) 'dot', and a volume weighted mean diameter D(4,3) 'dash'. The contact consists of hydrophobic PDMS of surface roughness 382 nm.

As we follow the Stribeck curve down in ηU, the system enters the mixed regime. Fig. 7(B) shows that for $\phi = 45\%$ suspension the onset of mixed lubrication occurs when the predicted central and minimum film thickness corresponds to the median ($D_{0.5} = 9$ μm) and the lowest ($D_{0.1} = 4.1$ μm) particle sizes respectively. This indicates that the speed at which the gap is similar to the particle size, the lubricant cannot be treated as a continuum and we suggest that the response no longer depends on the viscosity of the suspension but with that of the matrix phase, which transitions the system to the mixed-regime as the speed is decreased. Fig. 7(A) shows exactly that the friction for the 45% suspension partially overlaps with the Newtonian matrix in the mixed regime if one scales the entrainment speed using matrix viscosity ($\eta_{matrix}U$), which appears to be a controlling hydrodynamic factor in the mixed regime.

For the case of $\phi = 10\%$, the viscosity of suspension is very similar to that of matrix, i.e., $\eta_{matrix} \sim \eta_{suspension}$, and the onset of the mixed regime for both 10% suspension and the Newtonian matrix as shown in Fig. 7 occurs at similar values of entrainment speed. However, we still find evidence that support the hypothesis for the 'matrix-controlled' mixed regime. When examining the mixed lubrication for 'rough' surfaces (Fig. 3) for which the size of asperities is comparable with the size of particle, we observe significant differences in the mixed lubrication between the 10% suspension and the Newtonian matrix. If particles are present in the 'rough' contacts, which we believe they are, the results in Fig. 3 clearly illustrate their capacity to modulate the frication response in the mixed regime. By contrast, when examining the mixed lubrication for 'smooth' and 'medium'-rough surfaces (Fig. 3), we observe no difference between the suspension and the Newtonian matrix, which favours the hypothesis that particles may not be present in the gap to a tune necessary to effect friction response, and hence the matrix viscosity becomes a controlling hydrodynamic factor in the mixed regime. We note that the use of 'rough' surfaces presents its own limitations, since we observed large hysteresis between the curves recorded on the ascending and descending speed ramps. This hysteresis is probably due to the dynamic nature of particle entrapment into the contact, and may be partially responsible for the observed deviations from the Newtonian matrix in the mixed regime, as can be seen in Figs. 3 and 4.

Apart from the anomalously low boundary friction and the presence of the friction maximum prior to the onset of mixed lubrication, the tribological behaviour of particle suspension follows the Stribeck behaviour (Figs. 1 and 7). In fact, it is remarkable that Stribeck curves can be constructed for particle suspensions. The use of bulk viscosities to scale with the entrainment speed is rather unexpected, since the rheological behaviour inside and around the contact is not simple given high shear rates present in the gap and the potential for depletion of particles away from the shearing surfaces. Certainly, depletion affects viscosity measurements at high shear rates, although when this is taken into account, Davies and Stokes [28] did find that the viscosity of glass sphere suspensions followed the Quemada viscosity model [30] down to be very narrow gaps at high shear rates in a torsional parallel plate geometry, even when the gap is similar to the average particle size. Our results indicate that this seems to translate to elastohydrodynamic lubrication.

4.2. The mechanism of friction in the partial lubrication regime modulated by particles

In the mixed regime with decreasing U, the Stribeck curves for suspensions depart from the Newtonian master curve. The deviation depends on the particle phase volume and roughness of the substrate. We propose that the decrease in the hydrodynamic drag within the matrix-dominated mixed regime sets conditions favouring particle re-entry into the gap. (Please see the next section and Fig. 9 showing images of entrained particles). This re-entry manifests itself as a reduction in friction in the ηU-region below the mixed regime and down to the ηU values at the friction maximum. We call this region a partial lubrication regime; and we propose that the total friction force depends on relative contributions from the substrates (PDMS/PDMS) and particles-substrate (glass/PDMS) contact, as described in Eq. (1). In essence, with decreasing entrainment speed some PDMS/PDMS contacts are substituted with less frictious glass/PDMS contacts, which results in the overall decrease in the friction force. Note, the hollow glass spheres are made from borosilicate, which is hydrophilic (estimated contact angle ~30°[34]).

$$\mu_{TOTAL} = \mu_P(1-f) + \mu_G \cdot f \tag{1}$$

f is the fraction of the glass/PDMS asperity contacts, μ_P and μ_G are Stribeck curves for the PDMS/PDMS and glass/PDMS contacts respectively. f depends on surface roughness and particle size distribution, and it increases with increasing particle phase volume. A set criteria in this analysis is that at some entrainment speed (U^*), no particles are entrained into the gap; i.e. the system transitions into the matrix dominated mixed regime. A simple linear approximation yields the expression for the dependency of f on the entrainment speed:

$$f = f_0 - \frac{f_0}{U^*}U \tag{2}$$

f_0 is the maximum fraction of glass/PDMS contacts as the entrainment speed approaches zero. Substituting (2) into (1) yields an expression for μ_{TOTAL}:

$$\mu_{TOTAL} = \mu_P - f_0 \cdot \Delta\mu + \frac{f_0}{U^*} \cdot U \cdot \Delta\mu \tag{3}$$

where $\Delta\mu = \mu_P - \mu_G$. The results of simulations using Eq. (3) and experimental Stribeck curves for PDMS/PDMS and glass/PDMS contacts are shown in Fig. 8. One can clearly see that partial lubrication lines are in good agreement with the experimental data for $U > U_{\mu_{max}}$. The best fit to the data was achieved by using $f_0 = 0.55$ and $f_0 = 0.74$ for the 10% and 45% suspension respectively. The proposed mechanism, however, fails to reproduce a distinct maximum and the friction response in the boundary regime at $U < U_{\mu_{max}}$.

4.3. The mechanism of friction in the boundary regime modulated by particles

The position of the maximum, μ_{max}, for 45% suspensions at ~50 mm/s roughly coincides with the maximum reported by Gabriele et al. [16]. However unlike with soft hydrocolloid suspensions used by Gabriele

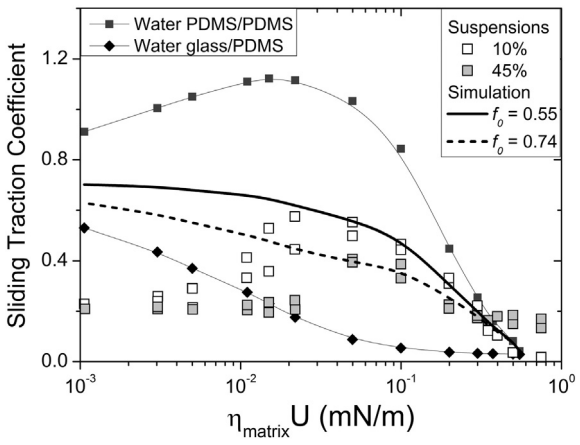

Fig. 8. Stribeck curves for particle suspensions (10% and 45% phase volume) in water and results of simulation using superposition approximation Eq. (3). The thick solid and dashed lines are calculated for the fraction of glass/PDMS contacts of 0.55 and 0.74 correspondingly. The data for PDMS/PDMS and glass/PDMS contacts in water are given for comparison. The contacts are hydrophobic PDMS with surface roughness 382 nm.

et al. or aggregating proteins [35], we do not expect that the observed maximum in the friction coefficient is associated with changes in the hydrodynamic conditions at the inlet or within the gap between rubbing surfaces. Even at very high phase volumes, the aggregation in the system of non-interacting particles like glass spheres used in this work is not observed.

An alternative mechanism of the friction maximum may be associated with the elastic hysteresis of the soft tribological contact, as predicted in modelling studies by Persson et al. [36,37]. However the magnitude of the drop in the friction coefficient at $U < U_{\mu_{max}}$ observed in our experiments is much larger than that predicted by the elastic hysteresis models. For the case of low SRR (Fig. 5), it is possible to estimate the friction coefficient due to elastic hysteresis losses using the model of Greenwood and Tabor [38], which yields $\mu_e \approx 0.014$. This estimate does not predict the total friction coefficient observed at low SRR as shown in Fig. 5. It is possible to suggest that for PDMS contacts the effects of adhesion may result in the increased contribution from the elastic hysteresis losses. We extend the elastic hysteresis model of Greenwood and Tabor [38] to include an adhesive Johnson, Kendall, Roberts (JKR) contact [39] in Eq. (4).

$$\mu_e = \alpha\left(\frac{\frac{3}{16R}a + M\frac{1}{\sqrt{2aR}}}{1 - 2M\sqrt{{}^{R}/_{a^3}}}\right) \tag{4}$$

α is loss factor, R is radius of the ball, a is the contact radius, and M is the material property factor, $M^2 = \frac{3}{2}\pi\gamma R \cdot \frac{1}{K} = F_{\text{pull-off}} \cdot \frac{3}{2}\left(\frac{1-\nu^2}{E}\right)$, which is effectively a pull-off force divided by the combined elastic modulus (E and ν are the PDMS Young's moduli and Poisson ratio respectively, γ is the work of adhesion). For a non-adhesive contact ($M = 0$), Eq. (4) reverts to the well-known formula derived by Greenwood and Tabor [38]. One can instantly see that the contribution from adhesion is rather minimal and for the case of PDMS material, leads to an increase in μ_e by ≤5%, which cannot explain results shown in Fig. 5. Therefore, an alternative mechanism is required to explain the modulation of friction by particles in water, and its function of U and the SRR. The results shown in Fig. 2 demonstrate that spherical particle suspensions even at phase volumes as low as 0.31% spheres are able to modulate the friction coefficient within the boundary regime. This ability of spherical particles to modulate friction at very low concentration suggests that particles are entrained into the contact and may even accumulate within the gap, where they assist in creating a barrier to asperity contact. We predict accumulation in the simple analysis presented in Section 4.2, whereby f significantly exceeds the value of the phase volume. As phase volume of particles is increased (Fig. 2), the friction coefficient decreases, indicating a greater number of particles carry the load. A constant friction coefficient for phase volumes beyond 5% indicates that no more than a monolayer of particles are present in the gap and 'excess' particles are excluded.

To support our analysis that particles are entrained into the contact at low ηU, a water immiscible fluorescent ink is imbedded into a PDMS ball, and tribology experiments are conducted at a constant speed of 5 mm/s for the 10% suspension. The microscopy images of the glass particles, taken after 5 min of rubbing, are shown in Fig. 9. It shows dye is transferred to those particles that pass through the contact and pressed between the PDMS surfaces. It should be noted that not all particles that are found within the area of rubbing had detectable fluorescent staining on them, which suggests that perhaps not all particles experience enough pressure for the dye to be transferred.

The mechanism by which particles modulate friction is deduced from the experiment presented in Fig. 5, where it is found that the sliding friction coefficient for the 45% particle suspension in a sliding contact equals the rolling friction coefficient using pure water. For the 10% suspension, we see a clear transition from sliding dominated contact (at 200% SRR) to the rolling dominated contact (≤100% SRR). We

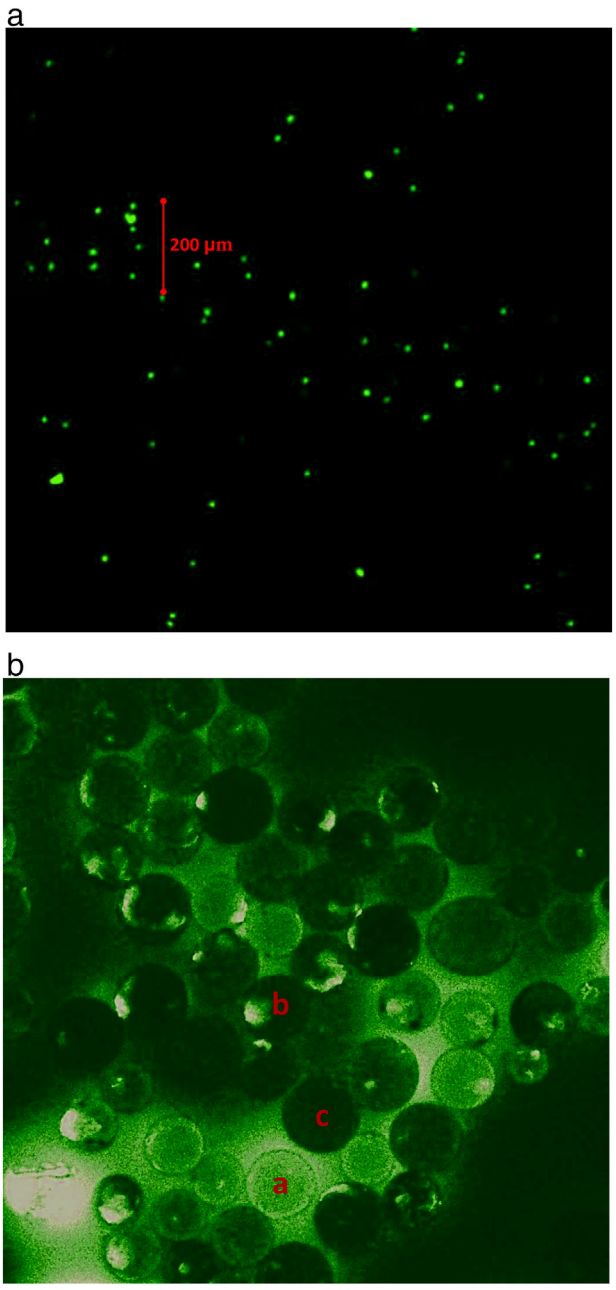

Fig. 9. (a) Image of PDMS disc showing transfer of dye from the PDMS ball to the PDMS disc after 5 min timed test in MTM (settings of F = 1N, SRR = 50%, U = 5 mm/s). (b) Image of glass particles showing dye staining; one can clearly see particles with homogeneous staining 'a', a patch-like staining 'b', and no staining 'c'.

therefore suggest that when the spherical particles are confined between PDMS at low ηU, a ball-bearing like action occurs that converts the sliding motion of substrates into the rolling of the particles. This effect results in the decrease in friction below that of the sliding contact between the glass and PDMS, as shown in Fig. 8.

4.4. On the entrainment of particles into tight gaps

The simple analysis presented above provides the insights that rationalises our observations and the Stribeck behaviour of the suspensions. However it remains quite puzzling how particles are entrained into the gap that, according to EHL theory, is smaller than the particles size. For soft contacts, we suggest that the deformation of the substrate, and consequently large contact area, is a key factor that enables such entrainment of particles and their subsequent rolling motion. However, we

observe no facilitation of friction for suspensions confined between hydrophilic contacts, as shown in Fig. 6. These contacts are equally soft and hence have similar contact area, and from purely mechanical and geometric considerations should allow particle entrainment. We propose that the probability of particle retention is dictated by the balance of forces acting to entrain or expel particles from the rubbing contact. In Fig. 10, we outline two scenarios for particle entrainment into adhesive and non-adhesive contact between compliant substrates.

In the adhesive contact between *hydrophobic* PDMS tribopair surfaces, particle-wall adhesion may restrict particle motion and lead to their mechanical confinement in the wedge between two surfaces forming the inlet [40]. We note that the expected gap between surfaces from hydrodynamic forces is ≤2 μm, estimated using the model of de Vicente et al. [26] from ηU; this is smaller than the particle diameter. Due to this geometric constraint, a particle cannot be entrained into the gap by the hydrodynamic drag ($\sim 6\pi U R_{particle} \approx 2nN$ for $U_{\mu_{max}} \approx 20$ mm/s). However, due to a large contact area ($a \sim 8$ mm^2), the perimeter of the wedge is of the order of a few millimetres (~2.5 mm, 45° arch of the inlet, Fig. 10(A)). This large area can accommodate a few hundred confined particles (~250). As each particle goes into the wedge, they act to deform the contact. The elastic force experienced at the surface of the PDMS at the wedge has two components: the vertical one, counter balanced by the force gauge of the tribometer, and the horizontal one, balanced by the friction force between the particle and PDMS surface. For an adhesive contact (between particles and surface), the total force acting on each particle is proportional to the adhesion force that is much larger than hydrodynamic drag (of the order of a few μN). At sufficiently low speeds, the particles may accumulate and as a collective ensemble facilitate wedging-in and further entrainment into the gap due to substrate deformation. Entrainment may also be facilitated by the roughness of PDMS tribopairs.

In the non-adhesive contacts between *hydrophilic* PDMS tribopair surfaces (Fig. 6), the entrainment of particles is controlled by the balance of the hydrodynamic drag, and the thin film drainage repulsion at the

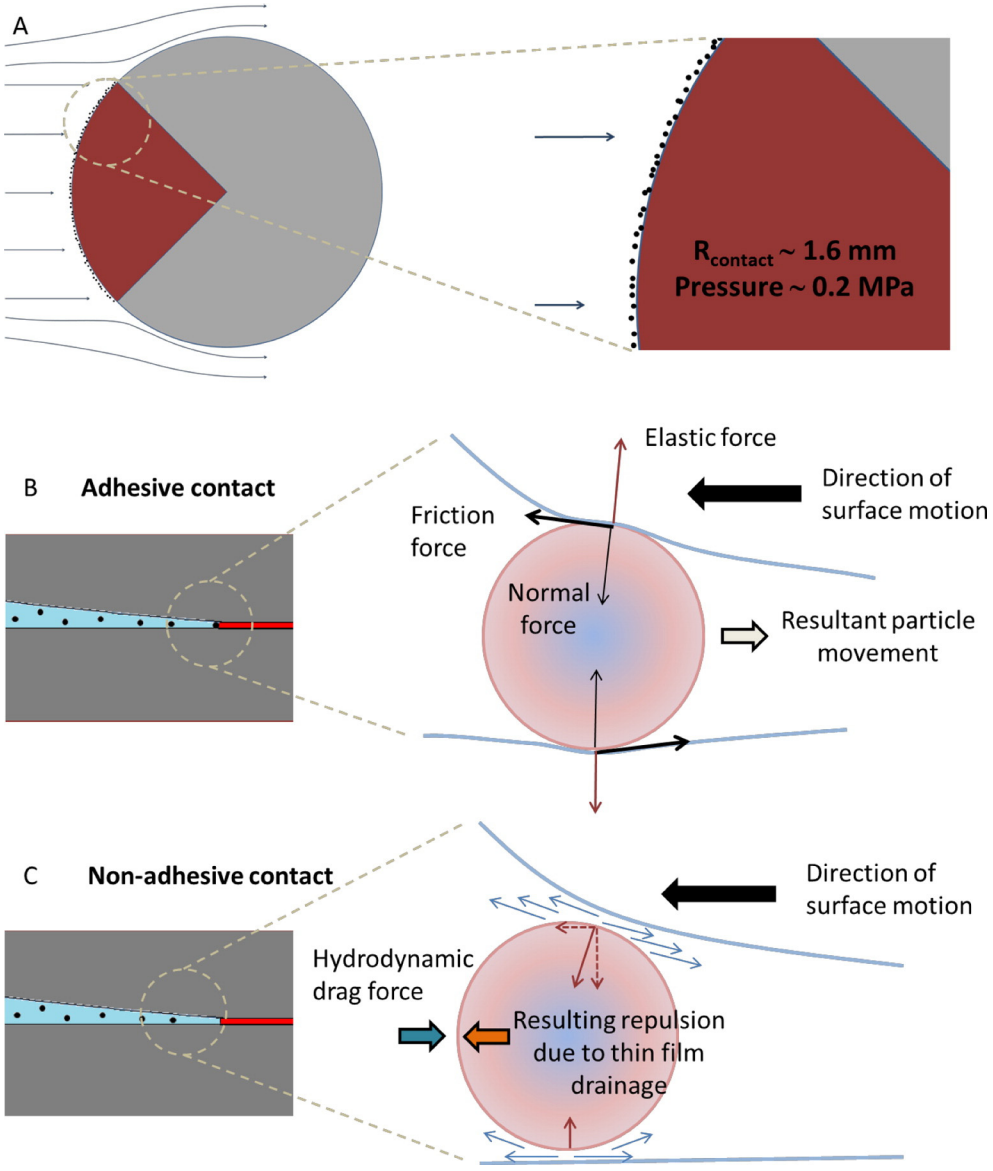

Fig. 10. (A) A scaled model of the PDMS-PDMS contact spot (top view). Due to compliant nature of PDMS the size of the contact is of order of few millimetres and pressures are of the order of 200 kPa (for the applied load of 1N). Many particles can accumulate around the perimeter of contact, especially where the vectors of fluid flow (arrows) come at high angles relative to the tangent of the contact line. The segment of the contact areas with high probability of particle entrapment is highlighted in red. (B) The side view of a wedge formed by 2 PDMS surfaces. A scaled model (left) and the model of forces (right) arising from particle–PDMS adhesion. For soft surfaces deformation results in higher adhesion which may result in the entrainment of the particles under sliding as well as rolling conditions. (C) A scaled model (left) and the model of forces (right) arising in the case of non-adhesive contact.

wedged-shaped inlet. Since both forces are linearly proportional to the speed, the effective thickness of the thin film between the PDMS surfaces and the glass particle is speed independent, and hence stays constant for a given shape of the wedge and the particle radius. The presence of such fluid film prevents the solid–solid contact between PDMS and glass particles to be established, which in turn inhibits particle entrainment.

5. Concluding remarks

We have investigated the behaviour of suspensions of hard glass spheres in a compliant lubricating contact. A novel aspect of our work has been to vary the viscosity of the aqueous matrix phase in order to probe the influence of the hard spheres (9 μm diameter) across the boundary, mixed and elasto-hydrodynamic lubrication regimes.

In general for hydrophobic surfaces we find the following. In the elasto-hydrodynamic regime, lubrication is dominated by the viscosity of the suspension provided the gap between tribopairs is larger the size of particles in the lubricant. As the speed and thus film thickness decreases, there is a transition corresponding to when the film thickness is similar to the size of the spheres. At this point, the suspension no longer behaves as a continuum and the tribological system 'jumps' to a mixed lubrication regime where the friction increases with decreasing speed. In this regime, multiplying the speed by the matrix viscosity leads to the same Stribeck curve for the suspensions as the matrix phase in the absence of particles. With further decrease in the entrainment speed, there is a departure from the matrix Stribeck curve corresponding to the junction between the mixed and boundary regimes. In the boundary regime, glass spheres lower the friction due to 'ball-bearing' like behaviour provided the surface roughness is low enough that entrainment of particles prevents PDMS-PDMS asperity contacts. However, for rough surfaces the system is more controlled by suspension properties (as a continuum) rather than the individual particles that appear to fail to provide sufficient barrier.

For hydrophobic surfaces, very low amounts of spheres are required to alter the boundary lubrication of the matrix phase. The friction curves measured at different slide–roll ratios and microscopic observations of the existence of a limited number of particles in the contact has given support to the suggestion that particles act as a single layer of ball bearings between the surfaces. We find that the boundary friction does not alter when phase volume is increased beyond 5%. In addition, we find that the boundary friction between hydrophilic surfaces increases with the presence of glass spheres, which is due to the lower rate of particle entrainment in the absence of adhesive interaction between glass and hydrophilic PDMS, which consequently nullifies the 'ball-bearing' effect. By the same token the absence of entrainment may modify the hydrodynamics of the inlet zone, which results in the increase friction.

We conclude that spherical particles have a profound effect on soft contact friction. It is clear that: only few particles are needed to affect tribological response; bulk rheology properties are dominant until the particle size is similar to the gap between rubbing substrates and/or surface roughness length scale; and spherical particles roll in a soft contact. These results provide fundamental insights into how particulate systems behave in rubbing soft-tribological contacts, and are particularly relevant to biotribological applications such as oral processing and in-use physics of skin creams and other personal care products. The results (and approach) will also allow interpretation of the many tribological studies currently being performed on food and personal care produces where complex friction curves are usually observed due to the multi-component and multiphase nature of these materials.

Acknowledgements

The majority of experiments in this study were performed and funded by the research laboratory of Unilever R&D Colworth, Bedford, UK. The authors thank Dr. Ann-Marie Williamson (Unilever) for her support and many helpful discussions. Mr. Robert Davies (University of Queensland) is acknowledged for his help with evaluation of the dyes used for PDMS staining, as well as for conducting preliminary tribological experiments with such stained surfaces. PDMS staining work was performed within the Queensland node of the Australian National Fabrication Facility, a company established under the National Collaborative Research Infrastructure Strategy to provide nano- and micro-fabrication facilities for Australia's researchers.

References

[1] J. de Vicente, J.R. Stokes, H.A. Spikes, Soft lubrication of model hydrocolloids, Food Hydrocoll. 20 (2006) 483–491.
[2] J. de Vicente, J.R. Stokes, H.A. Spikes, The frictional properties of newtonian fluids in rolling-sliding soft-EHL contact, Tribol. Lett. 20 (2005) 273–286.
[3] J.H.H. Bongaerts, K. Fourtouni, J.R. Stokes, Soft-tribology: lubrication in a compliant PDMS-PDMS contact, Tribol. Int. 40 (2007) 1531–1542.
[4] K. Timm, C. Myant, H. Nuguid, H.A. Spikes, M. Grunze, Investigation of friction and perceived skin feel after application of suspensions of various cosmetic powders, Int. J. Cosmet. Sci. 34 (2012) 458–465.
[5] E.H.A. de Hoog, J.F. Prinz, L. Huntjens, D.M. Dresselhuis, G.A. van Aken, Lubrication of oral surfaces by food emulsions: the importance of surface characteristics, J. Food Sci. 71 (2006) E337–E341.
[6] S. Lee, M. Heuberger, P. Rousset, N.D. Spencer, A tribological model for chocolate in the mouth: general implications for slurry-lubricated hard/soft sliding counterfaces, Tribol. Lett. 16 (2004) 239–249.
[7] S. Lee, M. Heuberger, P. Rousset, N.D. Spencer, Chocolate at a sliding interface, J. Food Sci. 67 (2002) 2712–2717.
[8] M. Godet, The 3rd-body approach—a mechanical view of wear, Wear 100 (1984) 437–452.
[9] G.T.Y. Wan, H.A. Spikes, The behvior of suspended solid particles in rolling and sliding elastohydrodynamic contacts, Tribol. Trans. 31 (1988) 12–21.
[10] D. Jiao, S. Zheng, Y. Wang, R. Guan, B. Cao, The tribology properties of alumina/silica composite nanoparticles as lubricant additives, Appl. Surf. Sci. 257 (2011) 5720–5725.
[11] K. Timm, C. Myant, H.A. Spikes, M. Grunze, Particulate lubricants in cosmetic applications, Tribol. Int. 44 (2011) 1695–1703.
[12] E. Imai, K. Hatae, A. Shimada, Oral perception of grittiness: effect of particle size and concentration of the dispersed particles and the dispersion medium, J. Texture Stud. 26 (1995) 561–576.
[13] M. Langton, A. Astrom, A.M. Hermansson, Influence of the microstructure on the sensory quality of whey protein gels, Food Hydrocoll. 11 (1997) 217–230.
[14] E. Imai, Y. Shimichi, I. Maruyama, A. Inoue, S. Ogawa, K. Hatae, et al., Perception of grittiness in an oil-in-water emulsion, J. Texture Stud. 28 (1997) 257–272.
[15] S.R. Oungoulian, S. Chang, O. Bortz, K.E. Hehir, K. Zhu, C.E. Willis, et al., Articular cartilage wear characterization with a particle sizing and counting analyzer, J. Biomech. Eng. Trans. ASME 135 (2013).
[16] A. Gabriele, F. Spyropoulos, I.T. Norton, A conceptual model for fluid gel lubrication, Soft Matter 6 (2010) 4205–4213.
[17] F. Chinas-Castillo, H.A. Spikes, Mechanism of action of colloidal solid dispersions, J. Tribol. Trans. ASME 125 (2003) 552–557.
[18] F. Chinas-Castillo, H.A. Spikes, The behavior of colloidal solid particles in elastohydrodynamic contacts, Tribol. Trans. 43 (2000) 387–394.
[19] J.A. Williams, A.M. Hyncica, Mechanisms of abrasive wear in lubricated contacts, Wear 152 (1992) 57–74.
[20] C. Cusano, H.E. Sliney, Dynamics of solid dispersions in oil during the lubrication of point contacts. 1. Molybdenum-disulfide, ASLE Trans. 25 (1982) 190–197.
[21] Y. Kusano, I.M. Hutchings, Modelling the entrainment and motion of particles in a gap: application to abrasive wear, Proc. Inst. Mech. Eng. J-J. Eng. Tribol. 217 (2003) 427–433.
[22] D.N. Allsopp, R.I. Trezona, I.M. Hutchings, The effects of ball surface condition in the micro-scale abrasive wear test, Tribol. Lett. 5 (1998) 259–264.
[23] R.I. Trezona, D.N. Allsopp, I.M. Hutchings, Transitions between two-body and three-body abrasive wear: influence of test conditions in the microscale abrasive wear test, Wear 225 (1999) 205–214.
[24] C. Cusano, H.E. Sliney, Dynamics of solid dispersions in oil during the lubrication of point contacts. 1. Graphite, ASLE Trans. 25 (1982) 183–189.
[25] A. Kumar, S.R. Schmid, W.R.D. Wilson, Particle behavior in two-phased lubrication, Wear 206 (1997) 130–135.
[26] J. de Vicente, J.R. Stokes, H.A. Spikes, Rolling and sliding friction in compliant, lubricated contact, Proc. Inst. Mech. Eng. J-J. Eng. Tribol. 220 (2006) 55–63.
[27] C. Myant, H.A. Spikes, J.R. Stokes, Influence of load and elastic properties on the rolling and sliding friction of lubricated compliant contacts, Tribol. Int. 43 (2010) 55–63.
[28] G.A. Davies, J.R. Stokes, Thin film and high shear rheology of multiphase complex fluids, J. Non-Newtonian Fluid Mech. 148 (2008) 73–87.
[29] G.A. Davies, J.R. Stokes, On the gap error in parallel plate rheometry that arises from the presence of air when zeroing the gap, J. Rheol. 49 (2005) 919–922.
[30] D. Quemada, Rheology of concentrated disperse systems and minimum energy-dissipation principle.1. Viscosity-concentration relationship, Rheol. Acta 16 (1977) 82–94.
[31] H.M. Shewan, J.R. Stokes, Analytically predicting the viscosity of hard sphere suspensions from the particle size distribution, J. of Non-Newtonian Fluid Mech. 222 (2015) 72–81.

[32] G.E. Yakubov, J. McColl, J.H.H. Bongaerts, J.J. Ramsden, Viscous boundary lubrication of hydrophobic surfaces by mucin, Langmuir 25 (2009) 2313–2321.
[33] R. Nilsson, R.S. Dwyer-Joyce, U. Olofsson, Abrasive wear of rolling bearings by lubricant borne particles, Proc. Inst. Mech. Eng. J-J. Eng. Tribol. 220 (2006) 429–439.
[34] R. Mohammadi, A. Amirfazli, Contact angle measurement for dispersed microspheres using scanning confocal microscopy, J. Dispers. Sci. Technol. 25 (2004) 567–574.
[35] J. Fan, C.W. Myant, R. Underwood, P.M. Cann, A. Hart, Inlet protein aggregation: a new mechanism for lubricating film formation with model synovial fluids, Proc. Inst. Mech. Eng. H-J. Eng. Med. 225 (2011) 696–709.
[36] B.N.J. Persson, M. Scaraggi, Theory of adhesion: role of surface roughness, J. Chem. Phys. 141 (2014).
[37] B.N.J. Persson, M. Scaraggi, On the transition from boundary lubrication to hydrodynamic lubrication in soft contacts, J. Phys. Condens. Matter 21 (2009).
[38] J.A. Greenwood, D. Tabor, The friction of hard sliders on lubricated rubber—the importance of deformation losses, Proc. Phys. Soc. Lond. 71 (1958) 989–1001.
[39] K.L. Johnson, K. Kendall, A.D. Roberts, Surface energy and contact of elastic solids, Proc. R. Soc. Lond. A Math. Phys. Sci. 324 (1971) (301-&).
[40] F. Hirano, S. Yamamoto, Four-ball test on lubricating oils containing solid particles, Wear 2 (1959) 349–363.